IXPE observations of the quintessential wind-accreting X-ray pulsar Vela X-1

Forsblom, S.V.; Poutanen, J.; Tsygankov, S.S.; Bachetti, M.; Di Marco, A.; Doroshenko, V.; ... ; Zane, S.

The Astrophysical Journal Letters, 947:L20 (10pp), 2023 April 20 https://doi.org/10.3847/2041-8213/acc391

IXPE Observations of the Quintessential Wind-accreting X-Ray Pulsar Vela X-1

Sofia V. Forsblom[1], Juri Poutanen[1,2], Sergey S. Tsygankov[1,2], Matteo Bachetti[3], Alessandro Di Marco[4], Victor Doroshenko[5], Jeremy Heyl[6], Fabio La Monaca[4], Christian Malacaria[7], Herman L. Marshall[8], Fabio Muleri[4], Alexander A. Mushtukov[9,10], Maura Pilia[3], Daniele Rogantini[8], Valery F. Suleimanov[5], Roberto Taverna[11], Fei Xie[4,12], Iván Agudo[13], Lucio A. Antonelli[14,15], Luca Baldini[16,17], Wayne H. Baumgartner[18], Ronaldo Bellazzini[16], Stefano Bianchi[19], Stephen D. Bongiorno[18], Raffaella Bonino[20,21], Alessandro Brez[16], Niccolò Bucciantini[22,23,24], Fiamma Capitanio[4], Simone Castellano[16], Elisabetta Cavazzuti[25], Chien-Ting Chen[26], Stefano Ciprini[15,27], Enrico Costa[4], Alessandra De Rosa[4], Ettore Del Monte[4], Laura Di Gesu[25], Niccolò Di Lalla[28], Immacolata Donnarumma[25], Michal Dovčiak[29], Steven R. Ehlert[18], Teruaki Enoto[30], Yuri Evangelista[4], Sergio Fabiani[4], Riccardo Ferrazzoli[4], Javier A. Garcia[31], Shuichi Gunji[32], Kiyoshi Hayashida[33,56], Wataru Iwakiri[34], Svetlana G. Jorstad[35,36], Philip Kaaret[18,37], Vladimir Karas[29], Takao Kitaguchi[30], Jeffery J. Kolodziejczak[18], Henric Krawczynski[38], Luca Latronico[20], Ioannis Liodakis[39], Simone Maldera[20], Alberto Manfreda[16], Frédéric Marin[40], Andrea Marinucci[25], Alan P. Marscher[35], Giorgio Matt[19], Ikuyuki Mitsuishi[41], Tsunefumi Mizuno[42], Michela Negro[43,44,45], Chi-Yung Ng[46], Stephen L. O'Dell[18], Nicola Omodei[28], Chiara Oppedisano[20], Alessandro Papitto[14], George G. Pavlov[47], Abel L. Peirson[28], Matteo Perri[14,15], Melissa Pesce-Rollins[16], Pierre-Olivier Petrucci[48], Andrea Possenti[3], Simonetta Puccetti[15], Brian D. Ramsey[18], John Rankin[4], Ajay Ratheesh[4], Oliver J. Roberts[26], Roger W. Romani[28], Carmelo Sgrò[16], Patrick Slane[49], Paolo Soffitta[4], Gloria Spandre[16], Rashid A. Sunyaev[2,50], Douglas A. Swartz[26], Toru Tamagawa[30], Fabrizio Tavecchio[51], Yuzuru Tawara[41], Allyn F. Tennant[18], Nicholas E. Thomas[18], Francesco Tombesi[27,52,53], Alessio Trois[3], Roberto Turolla[11,54], Jacco Vink[55], Martin C. Weisskopf[18], Kinwah Wu[54], and Silvia Zane[54]
(IXPE Collaboration)

[1] Department of Physics and Astronomy, FI-20014 University of Turku, Finland; juri.poutanen@utu.fi
[2] Space Research Institute of the Russian Academy of Sciences, Profsoyuznaya Str. 84/32, Moscow 117997, Russia
[3] INAF Osservatorio Astronomico di Cagliari, Via della Scienza 5, I-09047 Selargius (CA), Italy
[4] INAF Istituto di Astrofisica e Planetologia Spaziali, Via del Fosso del Cavaliere 100, I-00133 Roma, Italy
[5] Institut für Astronomie und Astrophysik, Universität Tübingen, Sand 1, D-72076 Tübingen, Germany
[6] Department of Physics and Astronomy, University of British Columbia, Vancouver, BC V6T 1Z1, Canada
[7] International Space Science Institute, Hallerstrasse 6, 3012 Bern, Switzerland
[8] MIT Kavli Institute for Astrophysics and Space Research, Massachusetts Institute of Technology, 77 Massachusetts Avenue, Cambridge, MA 02139, USA
[9] Astrophysics, Department of Physics, University of Oxford, Denys Wilkinson Building, Keble Road, Oxford OX1 3RH, UK
[10] Leiden Observatory, Leiden University, NL-2300RA Leiden, The Netherlands
[11] Dipartimento di Fisica e Astronomia, Università degli Studi di Padova, Via Marzolo 8, I-35131 Padova, Italy
[12] Guangxi Key Laboratory for Relativistic Astrophysics, School of Physical Science and Technology, Guangxi University, Nanning 530004, People's Republic of China
[13] Instituto de Astrofísicade Andalucía—CSIC, Glorieta de la Astronomía s/n, E-18008 Granada, Spain
[14] INAF Osservatorio Astronomico di Roma, Via Frascati 33, 00040 Monte Porzio Catone (RM), Italy
[15] Space Science Data Center, Agenzia Spaziale Italiana, Via del Politecnico snc, I-00133 Roma, Italy
[16] Istituto Nazionale di Fisica Nucleare, Sezione di Pisa, Largo B. Pontecorvo 3, I-56127 Pisa, Italy
[17] Dipartimento di Fisica, Università di Pisa, Largo B. Pontecorvo 3, I-56127 Pisa, Italy
[18] NASA Marshall Space Flight Center, Huntsville, AL 35812, USA
[19] Dipartimento di Matematica e Fisica, Università degli Studi Roma Tre, Via della Vasca Navale 84, I-00146 Roma, Italy
[20] Istituto Nazionale di Fisica Nucleare, Sezione di Torino, Via Pietro Giuria 1, I-10125 Torino, Italy
[21] Dipartimento di Fisica, Università degli Studi di Torino, Via Pietro Giuria 1, I-10125 Torino, Italy
[22] INAF Osservatorio Astrofisico di Arcetri, Largo Enrico Fermi 5, I-50125 Firenze, Italy
[23] Dipartimento di Fisica e Astronomia, Università degli Studi di Firenze, Via Sansone 1, I-50019 Sesto Fiorentino (FI), Italy
[24] Istituto Nazionale di Fisica Nucleare, Sezione di Firenze, Via Sansone 1, I-50019 Sesto Fiorentino (FI), Italy
[25] Agenzia Spaziale Italiana, Via del Politecnico snc, I-00133 Roma, Italy
[26] Science and Technology Institute, Universities Space Research Association, Huntsville, AL 35805, USA
[27] Istituto Nazionale di Fisica Nucleare, Sezione di Roma "Tor Vergata", Via della Ricerca Scientifica 1, I-00133 Roma, Italy
[28] Department of Physics and Kavli Institute for Particle Astrophysics and Cosmology, Stanford University, Stanford, California 94305, USA
[29] Astronomical Institute of the Czech Academy of Sciences, Boční II 1401/1, 14100 Praha 4, Czech Republic
[30] RIKEN Cluster for Pioneering Research, 2-1 Hirosawa, Wako, Saitama 351-0198, Japan
[31] California Institute of Technology, Pasadena, CA 91125, USA
[32] Yamagata University,1-4-12 Kojirakawa-machi, Yamagata-shi 990-8560, Japan
[33] Osaka University, 1-1 Yamadaoka, Suita, Osaka 565-0871, Japan
[34] International Center for Hadron Astrophysics, Chiba University, Chiba 263-8522, Japan
[35] Institute for Astrophysical Research, Boston University, 725 Commonwealth Avenue, Boston, MA 02215, USA
[36] Department of Astrophysics, St. Petersburg State University, Universitetsky pr. 28, Petrodvoretz, 198504 St. Petersburg, Russia
[37] Department of Physics and Astronomy, University of Iowa, Iowa City, IA 52242, USA
[38] Physics Department and McDonnell Center for the Space Sciences, Washington University in St. Louis, St. Louis, MO 63130, USA
[39] Finnish Centre for Astronomy with ESO, FI-20014, University of Turku, Finland
[40] Université de Strasbourg, CNRS, Observatoire Astronomique de Strasbourg, UMR 7550, F-67000 Strasbourg, France
[41] Graduate School of Science, Division of Particle and Astrophysical Science, Nagoya University, Furo-cho, Chikusa-ku, Nagoya, Aichi 464-8602, Japan
[42] Hiroshima Astrophysical Science Center, Hiroshima University, 1-3-1 Kagamiyama, Higashi-Hiroshima, Hiroshima 739-8526, Japan
[43] University of Maryland, Baltimore County, Baltimore, MD 21250, USA

[44] NASA Goddard Space Flight Center, Greenbelt, MD 20771, USA
[45] Center for Research and Exploration in Space Science and Technology, NASA/GSFC, Greenbelt, MD 20771, USA
[46] Department of Physics, University of Hong Kong, Pokfulam, Hong Kong
[47] Department of Astronomy and Astrophysics, Pennsylvania State University, University Park, PA 16801, USA
[48] Université Grenoble Alpes, CNRS, IPAG, F-38000 Grenoble, France
[49] Center for Astrophysics, Harvard & Smithsonian, 60 Garden Street, Cambridge, MA 02138, USA
[50] Max Planck Institute for Astrophysics, Karl-Schwarzschild-Str 1, D-85741 Garching, Germany
[51] INAF Osservatorio Astronomico di Brera, via E. Bianchi 46, I-23807 Merate (LC), Italy
[52] Dipartimento di Fisica, Università degli Studi di Roma "Tor Vergata," Via della Ricerca Scientifica 1, I-00133 Roma, Italy
[53] Department of Astronomy, University of Maryland, College Park, MD 20742, USA
[54] Mullard Space Science Laboratory, University College London, Holmbury St Mary, Dorking, Surrey RH5 6NT, UK
[55] Anton Pannekoek Institute for Astronomy & GRAPPA, University of Amsterdam, Science Park 904, 1098 XH Amsterdam, The Netherlands
Received 2022 November 27; revised 2023 March 2; accepted 2023 March 10; published 2023 April 19

Abstract

The radiation from accreting X-ray pulsars was expected to be highly polarized, with some estimates for the polarization degree of up to 80%. However, phase-resolved and energy-resolved polarimetry of X-ray pulsars is required in order to test different models and to shed light on the emission processes and the geometry of the emission region. Here we present the first results of the observations of the accreting X-ray pulsar Vela X-1 performed with the Imaging X-ray Polarimetry Explorer. Vela X-1 is considered to be the archetypal example of a wind-accreting, high-mass X-ray binary system, consisting of a highly magnetized neutron star accreting matter from its supergiant stellar companion. The spectropolarimetric analysis of the phase-averaged data for Vela X-1 reveals a polarization degree (PD) of $2.3\% \pm 0.4\%$ at the polarization angle (PA) of $-47\overset{\circ}{.}3 \pm 5\overset{\circ}{.}4$. A low PD is consistent with the results obtained for other X-ray pulsars and is likely related to the inverse temperature structure of the neutron star atmosphere. The energy-resolved analysis shows the PD above 5 keV reaching 6%–10% and a $\sim 90^\circ$ difference in the PA compared to the data in the 2–3 keV range. The phase-resolved spectropolarimetric analysis finds a PD in the range 0%–9% with the PA varying between -80° and 40°.

Unified Astronomy Thesaurus concepts: Pulsars (1306); Starlight polarization (1571); Neutron stars (1108); High mass x-ray binary stars (733); Magnetic fields (994); Accretion (14)

1. Introduction

Accreting X-ray pulsars (XRPs) harbor some of the strongest magnetic fields in the entire universe, which can be as large as several times 10^{12} G. The strong magnetic field channels accreting matter onto the polar regions at the neutron star (NS) surface, where it produces hot spots that are bright in the X-rays; these spots rotate in and out of the observer's line of sight, resulting in the appearance of pulsed X-ray emission. Highly magnetized XRPs represent unique laboratories, and much information is embedded in the interplay between the immense magnetic fields and the accretion flow. Observations of emission from accreting XRPs therefore constitute a substantial area of interest for theoretical models of matter interactions with ultrastrong magnetic fields, which cannot be replicated in terrestrial laboratories (see Mushtukov & Tsygankov 2022 for a recent review).

The magnetic field of the NS is the main cause for the polarized X-ray emission from accreting XRPs. The scattering of photons in a highly magnetized plasma is expected to result in a large degree of polarization of the emerging X-ray emission, up to 80% (Meszaros et al. 1988; Caiazzo & Heyl 2021). Meszaros et al. (1988) showed that linear X-ray polarization is strongly dependent on the geometry of the emission region and also that it varies with energy and pulse phase. X-ray polarimetric observations of accreting XRPs can therefore be used to probe the geometry of the emission region. The phase-resolved polarimetry can be used as a tool to constrain the viewing geometry and to distinguish between the models of their radiation.

A large window of opportunity to achieve significant observations of polarized X-ray emission opened up recently, thanks to the launch of the Imaging X-ray Polarimetry Explorer (IXPE; Weisskopf et al. 2022). IXPE is the first imaging X-ray polarimetric mission. For observations of XRPs, the strategy is to detect pulsations in the polarized emission, as well as to measure the polarization degree (PD) and polarization angle (PA) as a function of the pulse phase, which allows for the system geometry to be determined.

Vela X-1 (associated with the Uhuru source 4U 0900–40) is a high-mass X-ray binary (HMXB) discovered as one of the first X-ray sources at the early years of X-ray astronomy (Chodil et al. 1967) and remains one of the best-studied objects among NS HMXBs. It is one of the brightest, persistent XRPs chosen to be observed by IXPE. Vela X-1, located at a distance of about 2 kpc (Kretschmar et al. 2021), is often considered the quintessential wind accretor. It displays strong X-ray pulsations with a pulse period of 283 s (McClintock et al. 1976), variations with the orbital period of 8.964 days (Ulmer et al. 1972; van Kerkwijk et al. 1995), and eclipses lasting for about 2 days per orbit. The lower limit on the orbital inclination was obtained at $i = 73^\circ$ (van Kerkwijk et al. 1995).

Persistent wind-accreting XRPs are expected to have a different emission-region geometry as opposed to the disk-accreting Be/X-ray binaries. Additionally, polarization signatures are expected to be introduced by the scattering in the dense asymmetric wind. The main goal is therefore to study the accretion geometry for wind accretion and the properties of the dense stellar wind.

[56] Deceased.

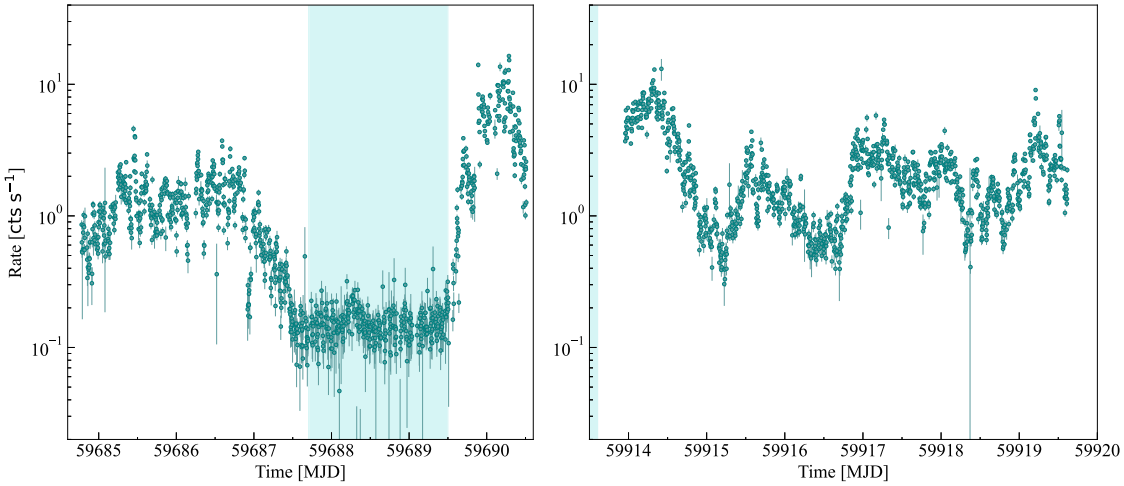

Figure 1. Background-corrected light curves of Vela X-1 in the 2–8 keV energy bands summed over the three DUs of IXPE for the first and second observations, shown in the left and right panels, respectively. The light-curve time bin value was set to ∼250 s. The time of the eclipse is marked by the blue shaded area.

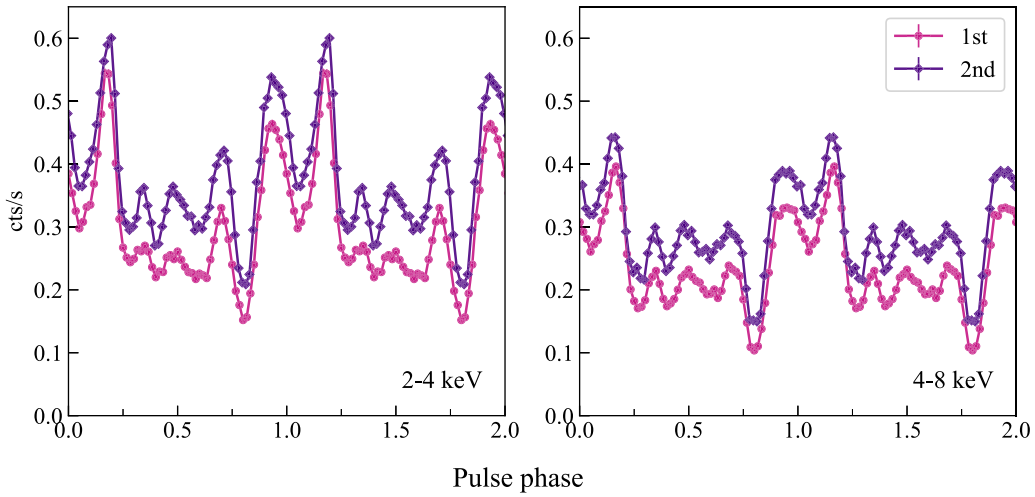

Figure 2. Pulse profiles of Vela X-1 as seen by IXPE in two different energy bands for the first and second observations, combined for DU1–3.

Quaintrell et al. (2003) have shown that the separation between the NS and its stellar companion, the B0.5Ib supergiant HD 77581 (also known as GP Vel), is only about 1.7 stellar radii, and therefore the NS is deeply embedded in the stellar wind of its companion star. The stellar companion has a mass-loss rate of $\sim 10^{-6} M_{\odot}$ yr^{-1} (Nagase et al. 1986). The average X-ray luminosity of the source is $\sim 4 \times 10^{36}$ erg s^{-1}. The luminosity is, however, strongly variable on all timescales, varying up to a factor of at least 20–30 (Soffitta et al. 2004; Kreykenbohm et al. 2008).

Observations of the cyclotron resonance scattering features in the spectra of XRPs provide a direct measurement of the magnetic field strength in the line-forming region. These features were first discovered in Vela X-1 by Kendziorra et al. (1992) by utilizing Mir-HEXE data, reporting a fundamental line around 25 keV and a first harmonic close to 50 keV. Evidence for these features was also given by Makishima & Mihara (1992), and they were further detailed by Kretschmar et al. (1996). Early observations with RXTE also confirmed this detection (Kretschmar et al. 1997). More recent observations of Vela X-1 by NuSTAR clearly detected the fundamental line at 25 keV together with a more prominent first harmonic at 55 keV and revealed a positive correlation between the harmonic line energy and the observed flux (Fürst et al. 2014). La Parola et al. (2016) confirmed a flux dependence of the first harmonic line energy and discovered its secular variation with time in the long-term data collected by Swift/BAT (see also Ji et al. 2019).

In this Letter, we present the first results of X-ray polarimetric observations of Vela X-1 by IXPE carried out on two separate occasions during 2022. In Section 2, the data used in the paper are described. Section 3 is devoted to the description of the results: the analysis of the phase-averaged, phase-resolved, and energy-resolved polarimetric data is given. Finally, the discussion and a short summary are presented in Section 4.

2. Data

IXPE is an observatory launched on 2021 December 9, as a NASA mission in partnership with the Agenzia Spaziale Italiana (ASI). IXPE consists of three telescope-detector systems that provide imaging polarimetry over a nominal 2–8 keV band at ∼30″ angular resolution (half-power diameter). Each one of the three grazing incidence telescopes is comprised of a mirror module assembly, which focuses the X-rays onto a corresponding focal plane polarization-sensitive gas pixel

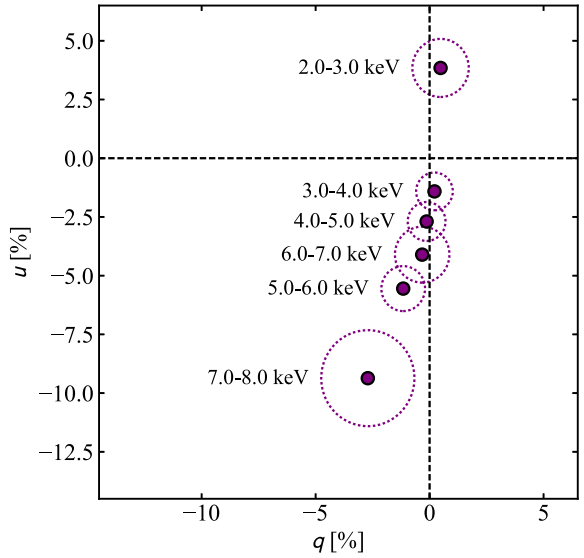

Figure 3. Energy dependence of the normalized Stokes parameters q and u for the phase-averaged data of the combined data set, obtained with the PCUBE algorithm.

electron tracking detector unit (DU). The detection principle is based on the photoelectric effect. All characteristics of each detected photon (sky coordinates, time of arrival, energy, and direction of the photoelectron) are measured simultaneously. A comprehensive description of the observatory, the instruments, and their performance is given by Soffitta et al. (2021) and Weisskopf et al. (2022).

IXPE observations of Vela X-1 were carried out between 2022 April 15–21 and November 30–December 6, with the total effective exposure of ≃280 ks and ≃270 ks, respectively. The data have been processed with the IXPEOBSSIM package version 30.2.1 (Baldini et al. 2022) using the CalDB released on 2022 November 17. The position offset correction and energy calibration were applied before the scientific analysis of the data. Source photons were collected using a circular region with a radius $R_{\rm src} = 70''$. The background region was chosen in the form of an annulus with inner and outer radii equal to $2R_{\rm src}$ and $4R_{\rm src}$, respectively. Data from the first observation were cleaned from events due to solar events, which have been identified by comparing the IXPE light curve with the one from the Geostationary Operational Environmental Satellite (GOES), then removing time intervals where the IXPE count rate in the background annular region was higher than the mean background value plus three times the rms of this count rate. The background makes up ∼3.6% and ∼2.2% of the total count rate of the source region in the 2–8 keV energy range for the first and second observations, respectively.

The barycorr tool from the FTOOLS package was used to correct the event arrival times to the barycenter of the solar system. This was followed by a correction of arrival times as it relates to the effects of binary motion using the orbital parameters obtained by the Fermi Gamma-ray Burst Monitor[57] for Vela X-1 and given in Table 1.

Stokes I energy spectra have been binned to have at least 30 counts per energy channel, and the same energy binning was applied to the energy spectra of Stokes parameters Q and U.

[57] https://gammaray.nsstc.nasa.gov/gbm/science/pulsars.html

Table 1
Orbital Parameters for Vela X-1 Adopted from the Fermi Gamma-ray Burst Monitor Project (dated 2021 January 30)

Parameter	Value	Unit
Orbital period	8.9642140	day
$T_{\pi/2}$	2459115.02085	Julian Ephemeris Date
$a_{\rm X} \sin i$	113.105	light-s
Longitude of periastron	162.33	deg
Eccentricity	0.0872	
Eclipse egress	0.12	
Eclipse ingress	0.92	

Table 2
Measurements of the Normalized Stokes Parameters q and u, PD, and PA for the Phase-averaged Data of Vela X-1 in Different Energy Bins Using the PCUBE Algorithm for the Combined Data Set

Energy (keV)	q (%)	u (%)	PD (%)	PA (deg)
2–3	0.5 ± 1.2	3.8 ± 1.2	3.9 ± 1.2	41.4 ± 9.1
3–4	0.2 ± 0.8	-1.4 ± 0.8	1.4 ± 0.8	-40.7 ± 16.1
4–5	-0.1 ± 0.8	-2.7 ± 0.8	2.7 ± 0.8	-46.4 ± 8.8
5–6	-1.2 ± 1.0	-5.6 ± 1.0	5.7 ± 1.0	-50.9 ± 4.8
6–7	-0.3 ± 1.2	-4.1 ± 1.2	4.1 ± 1.2	-47.3 ± 8.3
7–8	-2.7 ± 2.0	-9.4 ± 2.0	9.7 ± 2.0	-53.1 ± 6.0
2–8	-0.6 ± 0.5	-3.7 ± 0.5	3.7 ± 0.5	-49.9 ± 4.1

The energy spectra were fitted in the XSPEC package (Arnaud 1996) using χ^2 statistics, using the version 12 instrument response functions. The reported uncertainties are at the 68.3% confidence level (1σ), unless stated otherwise.

3. Results

3.1. Light Curve and Pulse Profile

The light curves from the first and second observations of Vela X-1 in the 2–8 keV energy range obtained with the IXPE observatory are shown in Figure 1. For the first observation of Vela X-1, the observing window can be separated into three parts: pre-eclipse (MJD 59,684.7–59,687.7), eclipse (MJD 59,687.7–59,689.5), and post-eclipse (MJD 59,689.5–59690.5). The post-eclipse count rate of the source was about 1 order of magnitude greater than the pre-eclipse source count rate. During the eclipse, which lasted about 2 days, the count rate dropped by 1 order of magnitude compared to the pre-eclipse value. For the following analysis, only pre- and post-eclipse data were included, i.e., only data outside of the eclipse.

A spin period of $P_{\rm spin} = 283.488(7)$ s and $P_{\rm spin} = 283.437(6)$ s were measured for Vela X-1 for the first and second observations, respectively, using phase-connection technique. The pulsed fraction in the 2–8 energy band, defined as $PF = (F_{\rm max} - F_{\rm min})/(F_{\rm max} + F_{\rm min})$, where $F_{\rm max}$ and $F_{\rm min}$ are the maximum and minimum count rates in the pulse profile, respectively, was determined as $PF = 53.3\% \pm 0.7\%$ for the first observation and as $PF = 48.1\% \pm 0.9\%$ for the second observation. The resulting pulse profiles for Vela X-1 in two separate energy bands are shown in Figure 2.

3.2. Polarimetric Analysis

First, the analysis of the polarimetric properties of Vela X-1 was carried out by using the PCUBE algorithm (xpbin tool) in

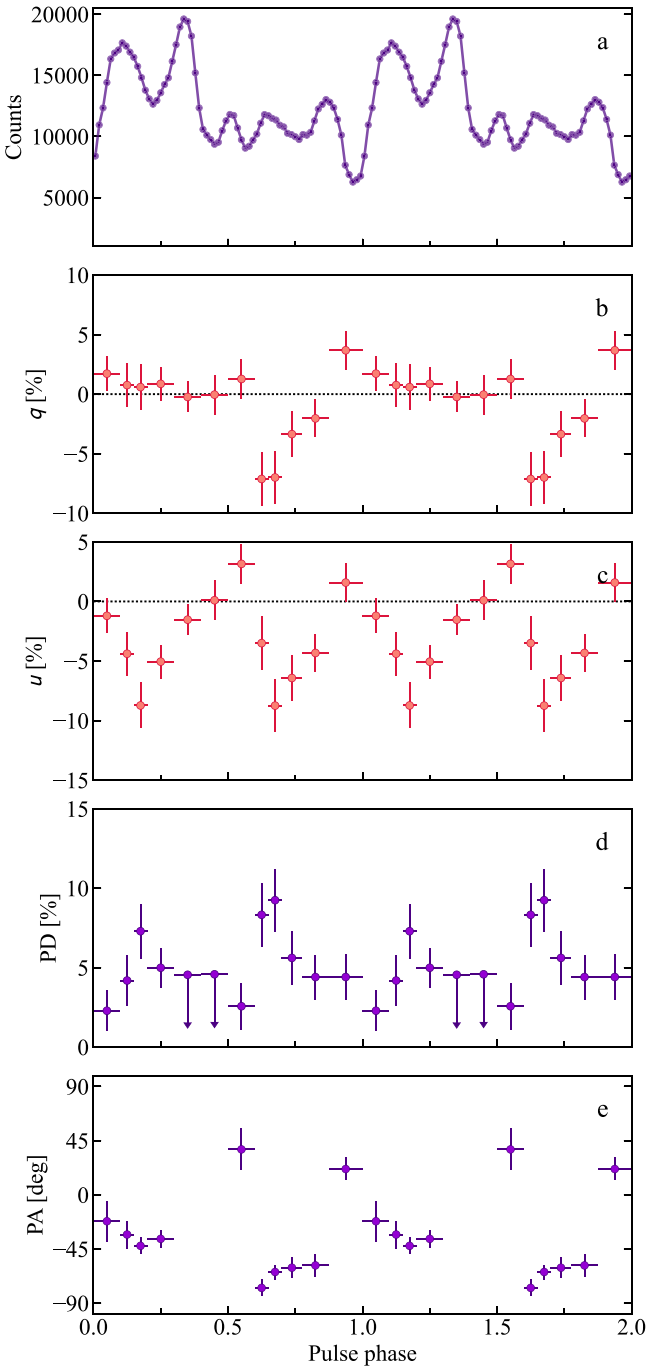

Figure 4. Phase-resolved analysis of Vela X-1 for the combined data set in the 2–7 keV range, combining data from all DUs. (a) Pulse profile. Panels (b) and (c) display the dependence of the Stokes q and u parameters, respectively, on the pulse phase, obtained for the phase-resolved polarimetric analysis utilizing the PCUBE algorithm. Panels (d) and (e) show the dependence of the PD and PA, respectively, on the pulse phase, obtained from the phase-resolved spectropolarimetric analysis using XSPEC. Upper limits (arrows) to the PD in panel (d) are at 99.73% (3σ) confidence level and are computed using a χ^2 with 1 degree of freedom.

the IXPEOBSSIM package, which is implemented according to the formalism by Kislat et al. (2015). The unweighted analysis has been used. We compute the normalized Stokes parameters, $q = Q/I$ and $u = U/I$, and the PD using the formula $\mathrm{PD} = \sqrt{q^2 + u^2}$ and ignoring the bias at low signal-to-noise ratios (Serkowski 1958; Simmons & Stewart 1985; Maier et al. 2014; Mikhalev 2018) and the $\mathrm{PA} = \frac{1}{2}\arctan(u/q)$ (measured counterclockwise on the sky from north to east).

In the entire IXPE energy band (2–8 keV), the average PD and PA are found to be $3.9\% \pm 0.9\%$ and $-51.^{\circ}5 \pm 6.^{\circ}5$, respectively, for the first observation. For the second observation, the average PD and PA are found to be $3.7\% \pm 0.7\%$ and $-48.^{\circ}9 \pm 5.^{\circ}2$, respectively.

Considering the similarities between the first and second observations, the data were combined into one single set of data in order to increase the statistics and further study the polarization properties of Vela X-1. In order to correctly phase-tag each event, the phase difference between the pulse profiles from the first and second observations was determined from cross correlation (using the implementation provided by the Python library NumPy). Using the PCUBE algorithm (xpbin tool) in the IXPEOBSSIM package, the average PD and PA are found to be $3.7\% \pm 0.5\%$ and $-49.^{\circ}9 \pm 4.^{\circ}1$, respectively, in the entire IXPE energy band.

We then studied the energy dependence of polarization by dividing the data into six energy bins. The PD is above the minimum detectable polarization at a 99% confidence level, MDP_{99} (Weisskopf et al. 2010), in all of the energy bins, except for the 3–4 keV bin, where the PD is below the MDP_{99}, and in this case, the PA is not well constrained (Table 2 and Figure 3). The energy-resolved analysis shows that at higher energies (above 5 keV) the PD reaches 6%–10% with the PA differing by $\sim 90^{\circ}$ from that below 3 keV.

Next, a phase-resolved polarimetric analysis was performed utilizing the PCUBE algorithm. The results in the 2–7 keV energy band are given in Table 3 and are shown in Figure 4 for the combined data set.

Then, the spectropolarimetric analysis was performed according to the following steps. Source I, Q, and U Stokes spectra were produced via the xpbin tools PHA1, PHA1Q, and PHA1U algorithms, producing a full data set comprised of nine spectra per observation, three for each DU. As the background region is dominated by source events, background subtraction is not applied (Di Marco et al. 2023). Here we also used unweighted analysis. The XSPEC package (version 12.12.1) (Arnaud 1996), which is a part of the standard high-energy astrophysics software suite HEASOFT, was used to study polarization as a function of energy. All 18 spectra were fitted simultaneously in XSPEC.

There are several phenomenological spectral models used to describe the spectral continuum of Vela X-1. However, it is well known that except for a soft excess below 3 keV, the X-ray emission below 10 keV can be well described by a simple absorbed power law with an iron line at 6.4 keV. Due to the restricted energy range covered by IXPE and the energy resolution of the instrument (Weisskopf et al. 2022), we used a simple model consisting of a power law affected by interstellar absorption (model tbabs with the abundances from Wilms et al. 2000) combined with the polconst polarization model, which assumes energy-independent PD and PA. In order to account for the soft excess below 3 keV, a partial covering fraction absorption (model tbpcf) was introduced as well, which applies an added column density to a fraction of the power law. The re-normalization constant, const, was used to account for the possibility of discrepancies between the different DUs, and for DU1 it was fixed to unity. The final model

```
tbabs × tbpcf × polconst × powerlaw × const
```

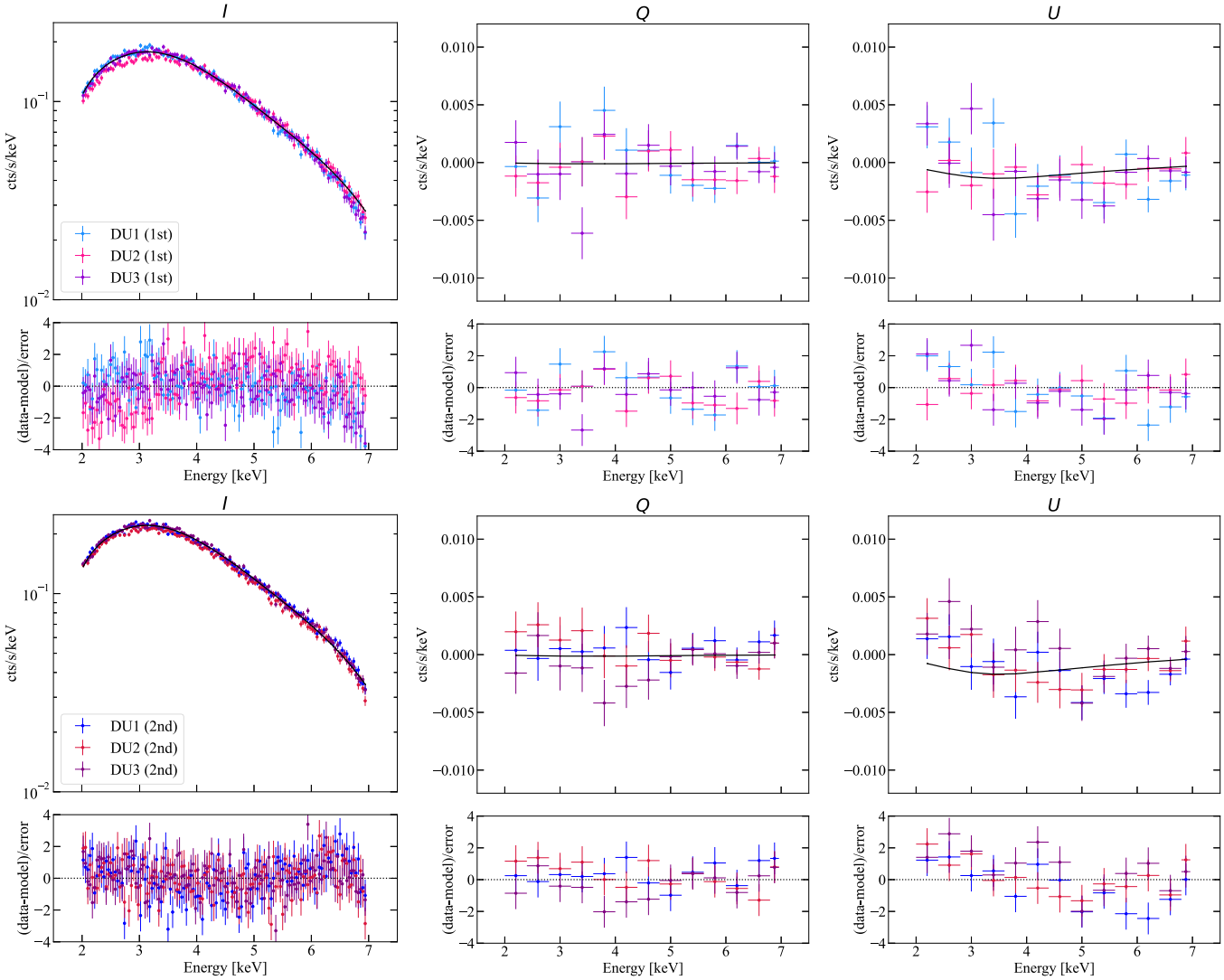

Figure 5. Stokes I, Q, and U energy distributions for the combined data set of Vela X-1 with the best-fit model superimposed for IXPE's DUs (upper larger panels in rows 1 and 3). The residuals between the best-fit model and the data are shown in the lower narrow panels of rows 2 and 4. Two upper and two lower rows correspond to the first and second observations, respectively, and are shown separately for clarity.

Table 3
Pulse-phase Dependence of the Normalized Stokes q and u Parameters for the Combined Data Set from the Polarimetric Analysis (2–7 keV) Using the PCUBE Algorithm and the Spectral Parameters, PD and PA, Obtained by the Spectropolarimetric Analysis

Phase	q (%)	u (%)	$N_{\rm H}$ (10^{22} cm^{-2})	$N_{\rm H,tbpcf}$ (10^{22} cm^{-2})	$f_{\rm cov}$	Photon Index	PD (%)	PA (deg)	χ^2/d.o.f.
0.000–0.100	1.7 ± 1.4	-1.2 ± 1.4	$6.0^{+0.7}_{-0.8}$	$23.0^{+1.8}_{-2.2}$	0.82 ± 0.02	$1.55^{+0.13}_{-0.16}$	2.3 ± 1.2	-22.0 ± 16.9	2160/2152
0.100–0.150	0.8 ± 1.8	-4.4 ± 1.8	$4.4^{+1.0}_{-1.4}$	$18.5^{+2.1}_{-2.0}$	$0.83^{+0.04}_{-0.03}$	1.26 ± 0.16	4.2 ± 1.6	-33.0 ± 11.3	2162/2029
0.150–0.200	0.6 ± 1.9	-8.7 ± 1.9	$4.9^{+1.2}_{-2.1}$	$18.4^{+3.2}_{-3.4}$	$0.77^{+0.07}_{-0.04}$	$0.96^{+0.19}_{-0.22}$	7.3 ± 1.7	-42.4 ± 6.8	2081/2011
0.200–0.300	0.9 ± 1.4	-5.1 ± 1.4	$3.8^{+0.8}_{-0.9}$	$19.9^{+2.1}_{-1.9}$	0.80 ± 0.02	$0.75^{+0.14}_{-0.13}$	5.0 ± 1.2	-36.6 ± 7.2	2284/2179
0.300–0.400	-0.2 ± 1.3	-1.5 ± 1.3	$4.0^{+0.9}_{-1.1}$	$16.5^{+1.7}_{-1.4}$	$0.81^{+0.04}_{-0.03}$	1.11 ± 0.11	<4.6	⋯	2304/2185
0.400–0.500	0.0 ± 1.7	0.1 ± 1.7	$4.2^{+0.8}_{-1.2}$	$20.5^{+2.5}_{-2.9}$	0.78 ± 0.03	1.08 ± 0.2	<4.6	⋯	2057/2086
0.500–0.600	1.3 ± 1.6	3.2 ± 1.6	$2.1^{+0.9}_{-1.2}$	$17.7^{+1.7}_{-1.7}$	0.83 ± 0.03	0.63 ± 0.13	2.6 ± 1.5	37.7 ± 17.2	2230/2116
0.600–0.650	-7.1 ± 2.2	-3.5 ± 2.2	$3.8^{+1.0}_{-1.5}$	$21.3^{+2.6}_{-3.0}$	0.82 ± 0.03	$0.98^{+0.19}_{-0.22}$	8.3 ± 2.0	-77.3 ± 6.9	1885/1858
0.650–0.700	-7.0 ± 2.2	-8.7 ± 2.2	$2.5^{+1.2}_{-1.8}$	$18.2^{+2.4}_{-2.1}$	0.84 ± 0.04	0.73 ± 0.18	9.2 ± 2.0	-64.2 ± 6.1	1934/1912
0.700–0.775	-3.4 ± 1.9	-6.4 ± 1.9	$0.6^{+1.5}_{-0.6}$	$15.3^{+2.0}_{-1.2}$	$0.85^{+0.02}_{-0.05}$	$0.30^{+0.15}_{-0.13}$	5.6 ± 1.6	-60.6 ± 8.7	2025/2038
0.775–0.875	-2.0 ± 1.6	-4.3 ± 1.6	$4.0^{+0.7}_{-1.0}$	$20.6^{+2.0}_{-2.2}$	0.81 ± 0.02	$1.05^{+0.14}_{-0.15}$	4.4 ± 1.4	-58.7 ± 9.2	2117/2134
0.875–1.000	3.7 ± 1.6	1.6 ± 1.6	$3.1^{+1.2}_{-2.1}$	$14.9^{+1.9}_{-1.7}$	$0.81^{+0.07}_{-0.05}$	$0.95^{+0.13}_{-0.15}$	4.4 ± 1.4	21.4 ± 9.5	2271/2092

Note. An upper limit to the PD at 99.73% (3σ) confidence level is computed using a χ^2 with one degree of freedom (d.o.f.).

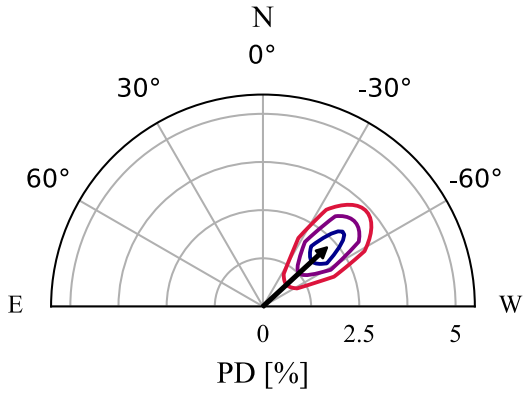

Figure 6. Polarization vector of Vela X-1 from the results of the phase-averaged spectropolarimetric analysis of the combined data set. Contours at 68.3%, 95.45%, and 99.73% confidence are shown in blue, purple, and red, respectively.

Table 4
Spectral Parameters for the Best-fit Model Obtained from the Phase-averaged Spectropolarimetric Analysis of the Combined Data Set

Parameter	Value	Unit
$N_{\rm H}$	3.8 ± 0.3	10^{22} cm^{-2}
$N_{\rm H,tbpcf}$	$18.5^{+0.7}_{-0.6}$	10^{22} cm^{-2}
$f_{\rm cov}$	0.80 ± 0.01	
const$_{\rm DU2}$	0.964 ± 0.003	
const$_{\rm DU3}$	0.923 ± 0.002	
Photon index	0.93 ± 0.04	
PD	2.3 ± 0.4	%
PA	-47.3 ± 5.4	deg
Flux$_{2-8\ \rm keV}$	$7.93^{+0.02}_{-0.06}$	10^{-10} erg cm^{-2} s^{-1}
Luminosity$_{2-8\ \rm keV}$	3.8×10^{35}	erg s^{-1} at $d = 2.0$ kpc
χ^2 (d.o.f.)	2640.19 (2222)	

was subsequently applied to both the phase-averaged and phase-resolved data. The spectral analysis was confined to the 2–7 keV energy band, ignoring photons above 7 keV due to remaining calibration uncertainties.

For the phase-averaged data, the results of the spectral fitting, including the best-fit model, are shown in Figure 5, and the best-fit model parameters are found in Table 4. The `steppar` command in XSPEC was used to create the confidence contours for the polarization measurements, and the resulting contour plots at 68.3%, 95.45%, and 99.73% confidence levels are presented in Figure 6. The results of the phase-averaged polarimetric analysis for the two different approaches give compatible results.

A wavy structure of the Stokes U parameter residuals in Figure 5 (see also Figure 3) indicates that polarization is energy dependent. Thus, we replaced the `polconst` polarization model with the `pollin` model, corresponding to a linear energy dependence of the PD and PA. For the `pollin` model we assumed a constant PA (ψ_1 in XSPEC; we fixed $\psi_{\rm slope} = 0$) and allowed the PD to vary with photon energy E (keV) as $\mathrm{PD}(E) = A_1 + A_{\rm slope}(E-1)$. This results in an improved fit ($\chi^2/\mathrm{d.o.f.} = 2608.51/2221$ with an F-test probability of 2.3×10^{-7}). The best-fit parameters are $A_1 = -5.3\% \pm 2.3\%$ and $A_{\rm slope} = (2.2\% \pm 0.6\%)$ keV^{-1}, and PA$=\psi_1 = -47.^\circ1 \pm 6.^\circ1$. The negative A_1 means that the PA at lower energies is rotated by 90° relative to the PA at higher energies, and the PD is zero at ≈3.4 keV. Such a model is able to describe the observed behavior of Stokes Q and U parameters in Figures 3 and 5.

For the phase-resolved spectropolarimetric analysis, I, Q, and U Stokes spectra were extracted for each phase bin individually, again utilizing the `xpbin` tools `PHA1`, `PHA1Q`, and `PHA1U` algorithms. The I, Q, and U Stokes spectra were fitted with the same model as utilized for the phase-averaged spectropolarimetric analysis, with the cross-calibration constants for DU2 and DU3 fixed to the values obtained for the phase-averaged analysis (see Table 4). The results of the phase-resolved spectropolarimetric analysis are summarized in Table 3, and confidence contours corresponding to each phase bin are shown in Figure 7.

A spectropolarimetric phase-averaged analysis done separately for the eclipse data did not find a significant polarization, with an upper limit to the PD of 25.1% at 99.73% confidence level. An intensity-resolved spectropolarimetric analysis performed on the combined data did not reveal a significant difference in polarization properties between different luminosity levels.

4. Discussion and Summary

XRPs are prime targets for X-ray polarimetric missions, where a high PD has been theoretically predicted because of the strong dependence of the primary radiation processes on the polarization of X-ray photons. The birefringence of highly magnetized plasma allows for the radiative transfer to be treated in terms of two normal polarization modes: the ordinary (O) and extraordinary (X) mode (Gnedin & Pavlov 1974). These two modes have different orientations in relation to the plane made up of the direction of the magnetic field and the momentum of photons. For O-mode photons, the electric vector oscillates mainly within the plane, while for X-mode photons the electric vector oscillations are mainly oriented perpendicular to the plane. Below the cyclotron energy the opacities of the polarization modes differ significantly where the opacity of the X-mode is largely reduced compared to that of the O-mode (Lai & Ho 2003), resulting in the predictions for PD as high as 80% (Meszaros et al. 1988; Caiazzo & Heyl 2021).

However, a significantly lower PD of only ∼2.3% detected for Vela X-1 in the IXPE data is in line with recent measurements done for other accreting XRPs (Her X-1, Doroshenko et al. 2022; Cen X-3, Tsygankov et al. 2022; 4U 1626–67, Marshall et al. 2022), where similar, relatively low PDs have been reported. The X-ray polarization of accreting XRPs greatly depends on the structure of the emission region (which is unknown), and most theoretical models mentioned here do not account yet for the temperature structure of the NS atmosphere, assuming instead a uniform temperature in the spectral-forming region. In the case of the above-mentioned XRPs, the contradiction between the observed and the theoretically predicted values of the PD was explained with a model of the NSatmosphere overheated by the accretion process.

The key factor for the depolarized emission in this model is a conversion of modes at the so-called vacuum resonance. In strong magnetic fields, both the plasma and the vacuum are birefringent, where vacuum birefringence is a fundamental QED effect. Generally speaking, the two effects (plasma and vacuum birefringence) tend to work against each other, and at vacuum resonance, they cancel out (Mészáros & Ventura 1978). This leads to a transformation of the normal modes of radiation

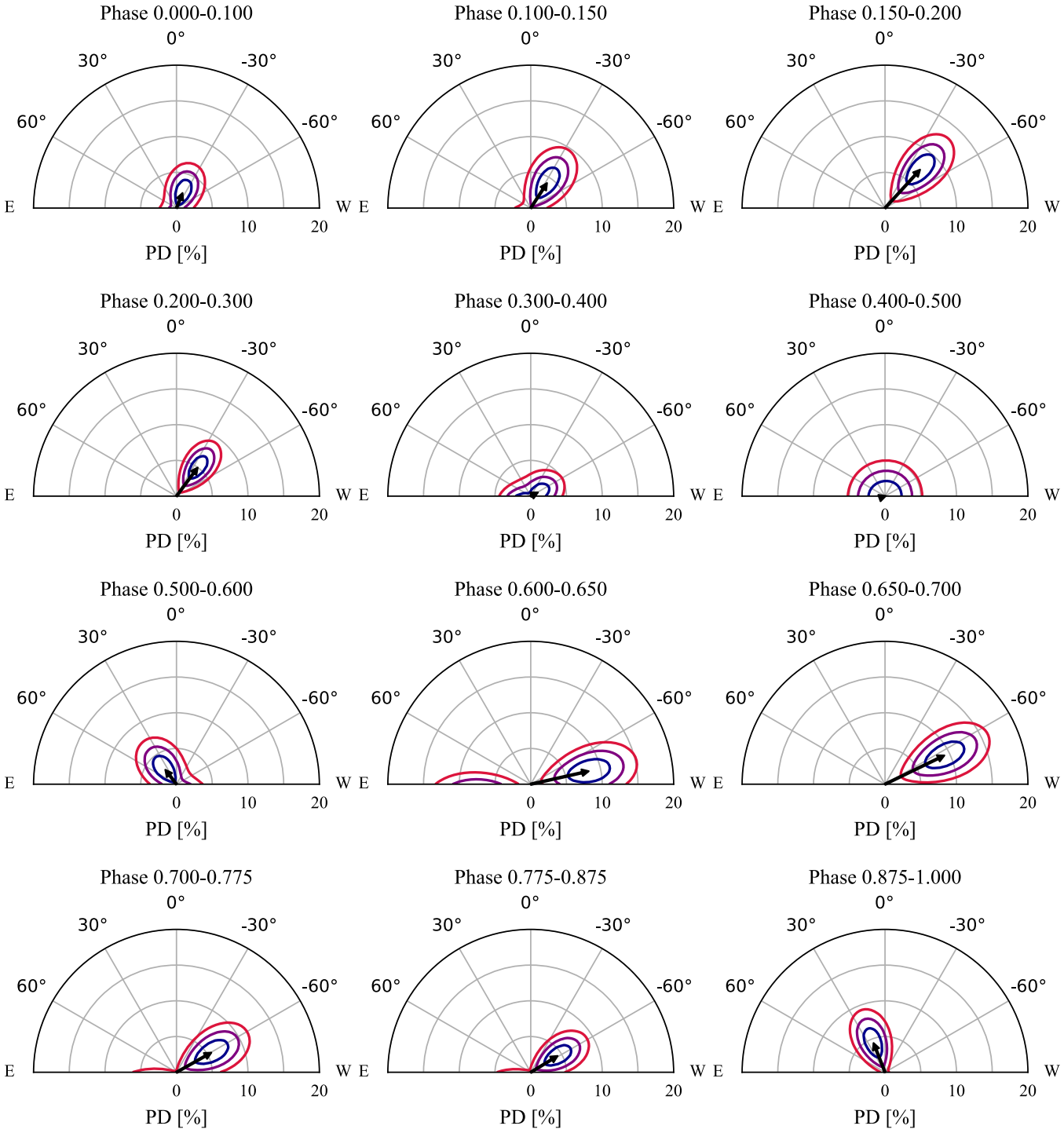

Figure 7. Polarization vectors of Vela X-1 from the results of the phase-resolved spectropolarimetric analysis of the combined data set. Contours at 68.3%, 95.45%, and 99.73% confidence are shown in blue, purple, and red, respectively.

and a loss of the linear PD. The vacuum resonance occurs at a plasma density $\rho_{\rm V} \approx 10^{-4} B_{12}^2 E_{\rm keV}^2$ [g cm^{-3}] for a given photon energy E (in keV) and local magnetic field strength $B_{12} = B/10^{12}$ G. This may result in a much smaller PD than normally predicted when considering the specific temperature structure of the atmospheres of accreting NSs. Doroshenko et al. (2022) have shown that a low PD of the X-ray radiation can be achieved if the point of vacuum resonance is located in an atmospheric transition layer with a strong temperature gradient. If the transition region is located at the border of the overheated upper atmospheric layer and the cooler underlying atmosphere, the low PD occurs as a result of the fast mode conversion (Gnedin et al. 1978). For the specific atmospheric thickness of $\sim$3 g cm^{-2}, corresponding to the Thomson optical depth around unity, a PD of the order of 10% can be achieved (Doroshenko et al. 2022). As lower PDs than previously predicted seem to be a staple of subcritical XRPs, theoretical models may well have to take into account the specific temperature structure of the NS atmosphere. On the other hand, the average observed luminosity for Vela X-1 is

$\sim 4 \times 10^{35}$ erg s^{-1}, roughly 2 orders of magnitude lower than the observed luminosities of Her X-1 and Cen X-3. Thus, it is rather puzzling that this scenario suggests a similar thickness of the overheated layer for a much smaller accretion rate; however, the key quantity here may be the proton-stopping depth (Zel'dovich & Shakura 1969; Nelson et al. 1993; Zane et al. 2000; González-Caniulef et al. 2019).

The low PD may also be a result of the strong variations of the PD and PA with energy (see Figure 3), considering the evident $\sim 90°$ difference in the PA below and above 3.5 keV. However, a complete and detailed analysis of the complicated energy dependence of the polarization properties of Vela X-1 is out of the scope of this Letter and is subject to future, more extensive work.

Finally, we can speculate that the observed small PD is a result of strong variations of the PA with the pulsar phase. The observed pulse profile has a very complicated shape, which is related either to the complex structure of the surface magnetic field or to the presence of a number of different components (see Tsygankov et al. 2022 for discussion). The present photon statistics allowed us to obtain significant detection of polarization in 9 out of 12 phase bins, while to resolve the variations of the PA, we likely needed many more bins.

The Imaging X-ray Polarimetry Explorer (IXPE) is a joint US and Italian mission. The US contribution is supported by the National Aeronautics and Space Administration (NASA) and led and managed by its Marshall Space Flight Center (MSFC), with industry partner Ball Aerospace (contract NNM15AA18C). The Italian contribution is supported by the Italian Space Agency (Agenzia Spaziale Italiana, ASI) through contract ASI-OHBI-2017-12-I.0, agreements ASI-INAF-2017-12-H0 and ASI-INFN-2017.13-H0, and its Space Science Data Center (SSDC) with agreements ASI-INAF-2022-14-HH.0 and ASI-INFN 2021-43-HH.0, and by the Istituto Nazionale di Astrofisica (INAF) and the Istituto Nazionale di Fisica Nucleare (INFN) in Italy. This research used data products provided by the IXPE Team (MSFC, SSDC, INAF, and INFN) and distributed with additional software tools by the High-Energy Astrophysics Science Archive Research Center (HEASARC), at NASA Goddard Space Flight Center (GSFC).

We acknowledge support from the RSF grant 19-12-00423 (SST), the Academy of Finland grants 333112, 349144, 349373, and 349906 (JP, SST), the German Academic Exchange Service (DAAD) travel grant 57525212 (VD, VFS), and the German Research Foundation (DFG) grant WE 1312/53-1 (VFS).

Facilities: IXPE.

Software: astropy (Astropy Collaboration et al. 2013, 2018), XSPEC (Arnaud 1996), IXPEOBSSIM (Baldini et al. 2022).

ORCID iDs

Sofia V. Forsblom https://orcid.org/0000-0001-9167-2790
Juri Poutanen https://orcid.org/0000-0002-0983-0049
Sergey S. Tsygankov https://orcid.org/0000-0002-9679-0793
Matteo Bachetti https://orcid.org/0000-0002-4576-9337
Alessandro Di Marco https://orcid.org/0000-0003-0331-3259
Victor Doroshenko https://orcid.org/0000-0001-8162-1105
Jeremy Heyl https://orcid.org/0000-0001-9739-367X
Fabio La Monaca https://orcid.org/0000-0001-8916-4156
Christian Malacaria https://orcid.org/0000-0002-0380-0041
Herman L. Marshall https://orcid.org/0000-0002-6492-1293
Fabio Muleri https://orcid.org/0000-0003-3331-3794
Alexander A. Mushtukov https://orcid.org/0000-0003-2306-419X
Maura Pilia https://orcid.org/0000-0001-7397-8091
Daniele Rogantini https://orcid.org/0000-0002-5359-9497
Valery F. Suleimanov https://orcid.org/0000-0003-3733-7267
Roberto Taverna https://orcid.org/0000-0002-1768-618X
Fei Xie https://orcid.org/0000-0002-0105-5826
Iván Agudo https://orcid.org/0000-0002-3777-6182
Lucio A. Antonelli https://orcid.org/0000-0002-5037-9034
Luca Baldini https://orcid.org/0000-0002-9785-7726
Wayne H. Baumgartner https://orcid.org/0000-0002-5106-0463
Ronaldo Bellazzini https://orcid.org/0000-0002-2469-7063
Stefano Bianchi https://orcid.org/0000-0002-4622-4240
Stephen D. Bongiorno https://orcid.org/0000-0002-0901-2097
Raffaella Bonino https://orcid.org/0000-0002-4264-1215
Alessandro Brez https://orcid.org/0000-0002-9460-1821
Niccolò Bucciantini https://orcid.org/0000-0002-8848-1392
Fiamma Capitanio https://orcid.org/0000-0002-6384-3027
Simone Castellano https://orcid.org/0000-0003-1111-4292
Elisabetta Cavazzuti https://orcid.org/0000-0001-7150-9638
Chien-Ting Chen https://orcid.org/0000-0002-4945-5079
Stefano Ciprini https://orcid.org/0000-0002-0712-2479
Enrico Costa https://orcid.org/0000-0003-4925-8523
Alessandra De Rosa https://orcid.org/0000-0001-5668-6863
Ettore Del Monte https://orcid.org/0000-0002-3013-6334
Laura Di Gesu https://orcid.org/0000-0002-5614-5028
Niccolò Di Lalla https://orcid.org/0000-0002-7574-1298
Immacolata Donnarumma https://orcid.org/0000-0002-4700-4549
Michal Dovčiak https://orcid.org/0000-0003-0079-1239
Steven R. Ehlert https://orcid.org/0000-0003-4420-2838
Teruaki Enoto https://orcid.org/0000-0003-1244-3100
Yuri Evangelista https://orcid.org/0000-0001-6096-6710
Sergio Fabiani https://orcid.org/0000-0003-1533-0283
Riccardo Ferrazzoli https://orcid.org/0000-0003-1074-8605
Javier A. Garcia https://orcid.org/0000-0003-3828-2448
Shuichi Gunji https://orcid.org/0000-0002-5881-2445
Wataru Iwakiri https://orcid.org/0000-0002-0207-9010
Svetlana G. Jorstad https://orcid.org/0000-0001-6158-1708
Philip Kaaret https://orcid.org/0000-0002-3638-0637
Vladimir Karas https://orcid.org/0000-0002-5760-0459
Jeffery J. Kolodziejczak https://orcid.org/0000-0002-0110-6136
Henric Krawczynski https://orcid.org/0000-0002-1084-6507
Luca Latronico https://orcid.org/0000-0002-0984-1856
Ioannis Liodakis https://orcid.org/0000-0001-9200-4006
Simone Maldera https://orcid.org/0000-0002-0698-4421
Alberto Manfreda https://orcid.org/0000-0002-0998-4953
Frédéric Marin https://orcid.org/0000-0003-4952-0835
Andrea Marinucci https://orcid.org/0000-0002-2055-4946
Alan P. Marscher https://orcid.org/0000-0001-7396-3332
Giorgio Matt https://orcid.org/0000-0002-2152-0916
Tsunefumi Mizuno https://orcid.org/0000-0001-7263-0296

Michela Negro https://orcid.org/0000-0002-6548-5622
Chi-Yung Ng https://orcid.org/0000-0002-5847-2612
Stephen L. O'Dell https://orcid.org/0000-0002-1868-8056
Nicola Omodei https://orcid.org/0000-0002-5448-7577
Chiara Oppedisano https://orcid.org/0000-0001-6194-4601
Alessandro Papitto https://orcid.org/0000-0001-6289-7413
George G. Pavlov https://orcid.org/0000-0002-7481-5259
Abel L. Peirson https://orcid.org/0000-0001-6292-1911
Matteo Perri https://orcid.org/0000-0003-3613-4409
Melissa Pesce-Rollins https://orcid.org/0000-0003-1790-8018
Pierre-Olivier Petrucci https://orcid.org/0000-0001-6061-3480
Andrea Possenti https://orcid.org/0000-0001-5902-3731
Simonetta Puccetti https://orcid.org/0000-0002-2734-7835
Brian D. Ramsey https://orcid.org/0000-0003-1548-1524
John Rankin https://orcid.org/0000-0002-9774-0560
Ajay Ratheesh https://orcid.org/0000-0003-0411-4243
Oliver J. Roberts https://orcid.org/0000-0002-7150-9061
Roger W. Romani https://orcid.org/0000-0001-6711-3286
Carmelo Sgrò https://orcid.org/0000-0001-5676-6214
Patrick Slane https://orcid.org/0000-0002-6986-6756
Paolo Soffitta https://orcid.org/0000-0002-7781-4104
Gloria Spandre https://orcid.org/0000-0003-0802-3453
Rashid A. Sunyaev https://orcid.org/0000-0002-2764-7192
Douglas A. Swartz https://orcid.org/0000-0002-2954-4461
Toru Tamagawa https://orcid.org/0000-0002-8801-6263
Fabrizio Tavecchio https://orcid.org/0000-0003-0256-0995
Allyn F. Tennant https://orcid.org/0000-0002-9443-6774
Nicholas E. Thomas https://orcid.org/0000-0003-0411-4606
Francesco Tombesi https://orcid.org/0000-0002-6562-8654
Alessio Trois https://orcid.org/0000-0002-3180-6002
Roberto Turolla https://orcid.org/0000-0003-3977-8760
Jacco Vink https://orcid.org/0000-0002-4708-4219
Martin C. Weisskopf https://orcid.org/0000-0002-5270-4240
Kinwah Wu https://orcid.org/0000-0002-7568-8765
Silvia Zane https://orcid.org/0000-0001-5326-880X

References

Arnaud, K. A. 1996, in ASP Conf. Proc. 101, Astronomical Data Analysis Software and Systems V, ed. G. H. Jacoby & J. Barnes (San Francisco, CA: ASP), 17
Astropy Collaboration, Price-Whelan, A. M., Sipőcz, A. M., et al. 2018, AJ, 156, 123
Astropy Collaboration, Robitaille, T. P., Tollerud, E. J., et al. 2013, A&A, 558, A33
Baldini, L., Bucciantini, N., Di Lalla, N., et al. 2022, SoftX, 19, 101194
Caiazzo, I., & Heyl, J. 2021, MNRAS, 501, 109
Chodil, G., Mark, H., Rodrigues, R., Seward, F. D., & Swift, C. D. 1967, ApJ, 150, 57
Di Marco, A., Soffitta, P., Costa, E., et al. 2023, AJ, 165, 143
Doroshenko, V., Poutanen, J., Tsygankov, S. S., et al. 2022, NatAs, 6, 1433
Fürst, F., Pottschmidt, K., Wilms, J., et al. 2014, ApJ, 780, 133
Gnedin, Y. N., & Pavlov, G. G. 1974, JETP, 38, 903
Gnedin, Y. N., Pavlov, G. G., & Shibanov, Y. A. 1978, SvAL, 4, 117
González-Caniulef, D., Zane, S., Turolla, R., & Wu, K. 2019, MNRAS, 483, 599
Ji, L., Staubert, R., Ducci, L., et al. 2019, MNRAS, 484, 3797
Kendziorra, E., Mony, B., Kretschmar, P., et al. 1992, in Proc. Yamada Conf. XXVIII, Frontiers Science Series, ed. Y. Tanaka & K. Koyama (Tokyo: Universal Academy Press), 51
Kislat, F., Clark, B., Beilicke, M., & Krawczynski, H. 2015, APh, 68, 45
Kretschmar, P., El Mellah, I., Martínez-Núñez, S., et al. 2021, A&A, 652, A95
Kretschmar, P., Pan, H. C., Kendziorra, E., et al. 1996, A&AS, 120, 175
Kretschmar, P., Pan, H. C., Kendziorra, E., et al. 1997, A&A, 325, 623
Kreykenbohm, I., Wilms, J., Kretschmar, P., et al. 2008, A&A, 492, 511
La Parola, V., Cusumano, G., Segreto, A., & D'Aì, A. 2016, MNRAS, 463, 185
Lai, D., & Ho, W. C. 2003, PhRvL, 91, 071101
Maier, D., Tenzer, C., & Santangelo, A. 2014, PASP, 126, 459
Makishima, K., & Mihara, T. 1992, in Proc. Yamada Conf. 23, XXVIII, Frontiers Science Series, ed. Y. Tanaka & K. Koyama (Tokyo: Universal Academy Press), 23
Marshall, H. L., Ng, M., Rogantini, D., et al. 2022, ApJ, 940, 70
McClintock, J. E., Rappaport, S., Joss, P. C., et al. 1976, ApJL, 206, L99
Meszaros, P., Novick, R., Szentgyorgyi, A., Chanan, G. A., & Weisskopf, M. C. 1988, ApJ, 324, 1056
Mészáros, P., & Ventura, J. 1978, PhRvL, 41, 1544
Mikhalev, V. 2018, A&A, 615, A54
Mushtukov, A., & Tsygankov, S. 2022, arXiv:2204.14185
Nagase, F., Hayakawa, S., Sato, N., Masai, K., & Inoue, H. 1986, PASJ, 38, 547
Nelson, R. W., Salpeter, E. E., & Wasserman, I. 1993, ApJ, 418, 874
Quaintrell, H., Norton, A. J., Ash, T. D. C., et al. 2003, A&A, 401, 313
Serkowski, K. 1958, AcA, 8, 135
Simmons, J. F. L., & Stewart, B. G. 1985, A&A, 142, 100
Soffitta, P., Baldini, L., Bellazzini, R., et al. 2021, AJ, 162, 208
Staubert, R., Kreykenbohm, I., Kretschmar, P., et al. 1992, in ESA Spec. Publ. 552, V INTEGRAL Workshop, the INTEGRAL Universe, ed. V. Schoenfelder, G. Lichti, & C. Winkler, 259
Tsygankov, S. S., Doroshenko, V., Poutanen, J., et al. 2022, ApJL, 941, L14
Ulmer, M. P., Baity, W. A., Wheaton, W. A., & Peterson, L. E. 1972, ApJL, 178, L121
van Kerkwijk, M. H., van Paradijs, J., Zuiderwijk, E. J., et al. 1995, A&A, 303, 483
Weisskopf, M. C., Elsner, R. F., & O'Dell, S. L. 2010, Proc. SPIE, 7732, 77320E
Weisskopf, M. C., Soffitta, P., Baldini, L., et al. 2022, JATIS, 8, 026002
Wilms, J., Allen, A., & McCray, R. 2000, ApJ, 542, 914
Zane, S., Turolla, R., & Treves, A. 2000, ApJ, 537, 387
Zel'dovich, Y. B., & Shakura, N. I. 1969, SvA, 13, 175